

**Thomas Gomes dos Santos<sup>1\*</sup>, André Rosiak<sup>1</sup>, Diego Pacheco Wermuth<sup>1</sup>, Lirio Schaeffer<sup>1</sup>**

<sup>1</sup> *Metal Forming Innovation Center (CBCM), Universidade Federal do Rio Grande do Sul (UFRGS), Porto Alegre, Brazil*

\* *thomasgomesdossantos@gmail.com*

## **IMAGE ANALYSIS APPLIED TO MONITORING THE HOT OPEN DIE FORGING PROCESS WITH DROP HAMMER**

### **ABSTRACT**

In gravity drop hammer forging, the ram is lifted to a certain height and then released. During the downward motion, the hammer is accelerated by gravity and strikes the workpiece. The operational environment of these machines presents adverse conditions, such as extreme temperatures, high impact velocity, and intense energy generation. These aspects make the instrumentation of these machines highly challenging, leading to the use of theoretical models to describe their dynamic behavior. However, these models involve simplifications that reduce the accuracy of the analyses. This study aims to evaluate the efficiency of Digital Image Correlation (DIC) as a monitoring tool for the hot forging process of AA 6351 aluminum alloy using a drop hammer. Digital Image Correlation allows for the quantitative analysis of the evolution of the workpiece deformation during the process, providing valuable data on process and machine performance. The results obtained demonstrate that Digital Image Correlation is a promising approach for monitoring the hot forging process with a drop hammer, with the potential to enhance the quality of the final product and process efficiency.

**Keywords:** *digital image correlation; forging; monitoring; drop hammer*

### **INTRODUCTION**

Drop hammer forging is a versatile and cost-effective equipment recognized for enhancing the metallurgical properties of various materials, including nickel-based superalloys used in critical applications such as turbine disc production. This technology, involving multiple impact blows between dies, is particularly employed for hot forging of small batches, prominently in the aerospace industry [1, 2]. However, the major limitation of drop hammers is energy restriction. During a working blow, deformation occurs until the total kinetic energy is dissipated through the plastic deformation of the workpiece material and elastic deformation of the machine itself [1].

Forging with drop hammers is characterized by high deformation speeds, reaching up to 200 1/s [3]. Deformation speed significantly influences the metallurgical properties of the final piece and, in combination with other parameters, determines the quality of the end product. Therefore, the analysis and control of these parameters are crucial during forging operations.

Forging operations, especially with hammers, take place under severe conditions.

Extreme temperatures, severe impacts, and high vibration make process instrumentation extremely challenging. For this reason, theoretical models are commonly used to describe the dynamic behavior of the machine. However, these models involve various simplifications that reduce the accuracy of analyses. Consequently, significant efforts have been made to enhance the analysis and control techniques of drop hammer forging processes.

In this context, the use of image-based sensors becomes attractive. This approach does not require physical contact between the sensor element and the analyzed object. This ensures sensor integrity without compromising precision in recordings. Camera systems are already widely used in the control of sheet metal forming processes. Images from different points of the process are utilized, for example, to assess the piece's quality and instantly measure piece dimensions [4]. Image analysis has also been proposed for part measurement in forging processes [5]. A system based on machine vision techniques integrated into a mechatronic system for automating the inspection of hot-forged parts was developed by [5]. The system utilizes six cameras and statistical analysis to determine whether a part can be approved or rejected. Experimental results validated the application of the proposed method for measuring parts under real factory floor conditions. In the study by [6], a high-speed camera was used in combination with a load cell to obtain rheological results of deformed copper in a drop hammer. Stress and strain values were analytically calculated using both techniques independently to generate the material's flow curve. This approach proved successful in characterizing the process kinematics. Different types of sensors were employed by [7] to measure displacement and force in the upsetting of copper using a high-speed screw press. The authors demonstrated that laser sensors have limitations in measuring the dynamic behavior of the forging process. According to the authors, predicting the forming force accurately is possible based on the rheological behavior and material deformation [7]. This study aims to evaluate the efficiency of Digital Image Correlation (DIC) as a monitoring tool for the hot drop hammer forging process. In the proposed approach, a high-speed camera, a conventional camera, a thermal camera, and a load cell are used to monitor the upsetting process of the AA6351 aluminum alloy performed at 300°C.

## MATERIALS AND METHODS

Figure 1 illustrates the schematic drawing of the experimental procedure. Cylindrical specimens ( $\text{Ø}15 \times 24 \text{mm}$ ) of the AA6351 aluminum alloy were heated to 300°C in a resistance furnace for 30 minutes and promptly transferred to flat dies mounted in a gravity drop hammer. The dies were pre-coated with a layer of graphitic liquid lubricant. The bottom die was mounted on a load cell for measuring the forming force. For load signal recording, an analog data acquisition module (HBM© - SPIDER 8®) and CATMAN® software were utilized.

Figure 2 shows the experimental setup. The DIC analysis of the experimental procedure was divided into two stages, as depicted in Figure 3.

STEP I involves the hammer drop until the moment the upper die touches the upper surface of the billet. Monitoring this stage was carried out using a Canon t5i camera and a calibration scale. From the obtained data, the displacement derivative can be calculated, and the impact velocity determined. The analysis of this stage was aided by the free software TRACKER®.

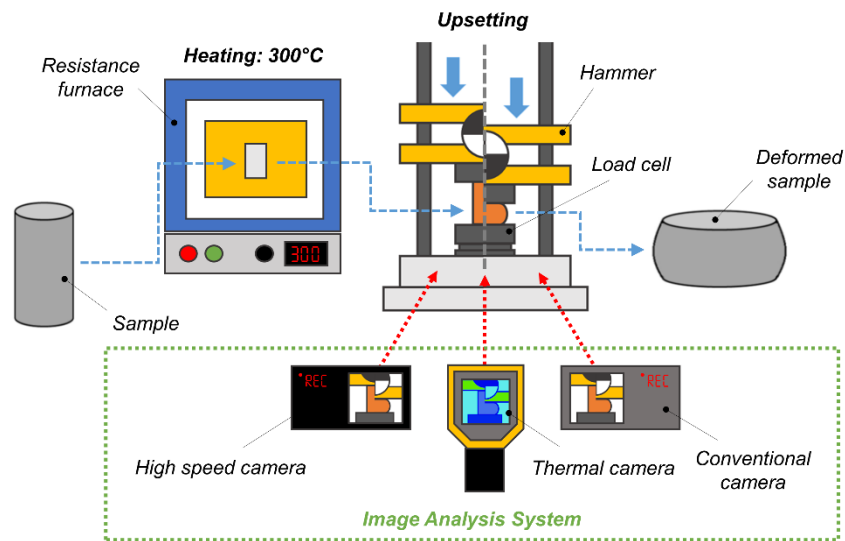


Fig. 1. Schematic drawing of the experimental procedure

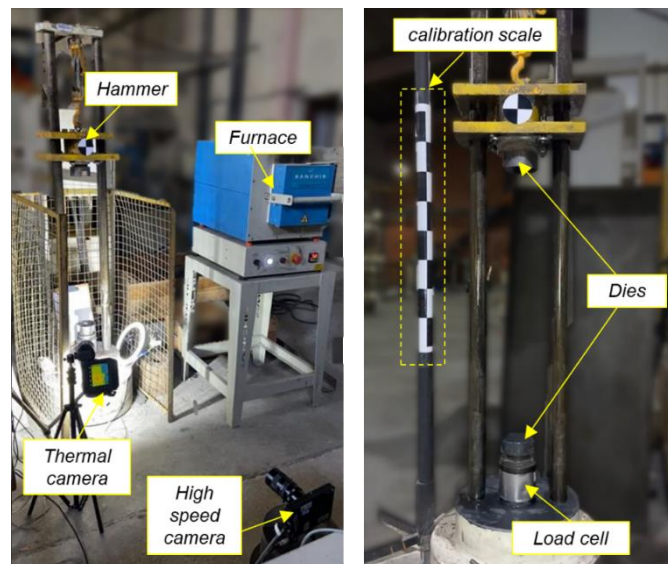


Fig. 2. Experimental setup assembly

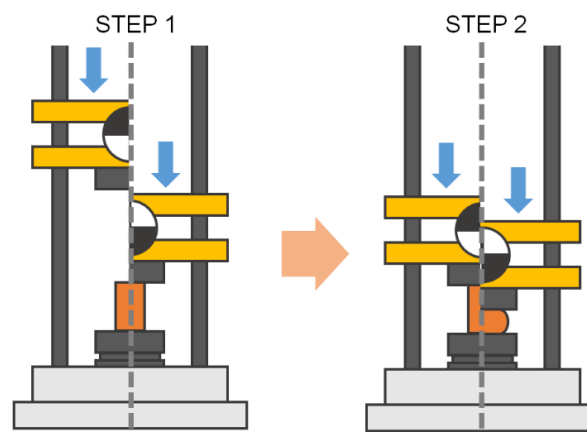


Fig. 3. Stages of image analysis

STEP II involves the deformation of the billet. This stage was recorded using a high-speed camera FASTEC-IL3-271 and a Flir® T530 thermal camera. The data obtained in STEP II were used to calculate the main parameters of the upsetting process.

The gravity hammer used has a maximum height of 1 m, and the mass of the upper hammer system is 40 kg. The calculation of the forming force requires knowledge of the rheological properties of the working material. In deformation at elevated temperatures, as in this study, the yield stress depends not only on deformation but is also strongly influenced by the strain rate. The commonly used mathematical form to describe these relationships is the Hensel-Spittel Equation [8]:

$$k_f = A \cdot e^{m_1 \cdot \vartheta} \cdot \varphi^{m_2} \cdot \dot{\varphi}^{m_3} \quad (1)$$

Where  $A$ ,  $m_1$ ,  $m_2$  and  $m_3$  are material constants that must be experimentally determined,  $\vartheta$  temperature,  $\varphi$  equivalent plastic strain and  $\dot{\varphi}$  strain rate. Table 1 presents the Hensel-Spittel parameters for the AA6351 alloy [9]. The data obtained from the proposed monitoring approach were compared to results from finite element analysis. A 2D numerical simulation of the process was performed using QFORM software. To reduce computational effort, only the billet's behavior was assigned as viscoplastic. The tools were considered rigid. The parameters of the Hensel-Spittel Equation (Table 1) were introduced into the numerical models. Table 2 lists the boundary conditions used in the numerical model.

**Table 1.** Parameters of the Hensel-Spittel Equation for the AA 6351 alloy [9]

A [MPa]	303.5
$m_1$ [-]	-0.0043
$m_2$ [-]	0.103
$m_3$ [-]	0.057

**Table 2.** Input data used in the numerical model

Analysis type	2D viscoplastic
Number of elements	800
Element size	0.47 mm
Element type	4 - isoparametric quadrilateral elements
Tool temperature	23 °C
Initial workpiece temperature	300 °C
Heat transfer coefficient	10000 W/m <sup>2</sup> K
Thermal conductivity	180 W/m-K
Specific heat	6351 J/(kg.K)
Modulus of Elasticity	68.9 GPa
Friction factor	m = 0.3

The value defined for the coefficient of friction was determined by ring compression test method under the same temperature and lubrication conditions used in the upsetting experiments.

## RESULTS

For the analysis of the hammer falling motion, the free software Tracker was used. The software tracks an object in a video (Figure 4), extracting kinetic parameters from the motion. From the video capture and subsequent data processing, data on the hammer's velocity,

displacement, and acceleration during the fall were acquired. The values obtained during the experiments can be observed in Figures 5 and 6.

Based on the obtained displacement and velocity data, it can be concluded that during the falling motion, the hammer maintained an increasing velocity until reaching its maximum value of 3.271 m/s at 0.433 s.

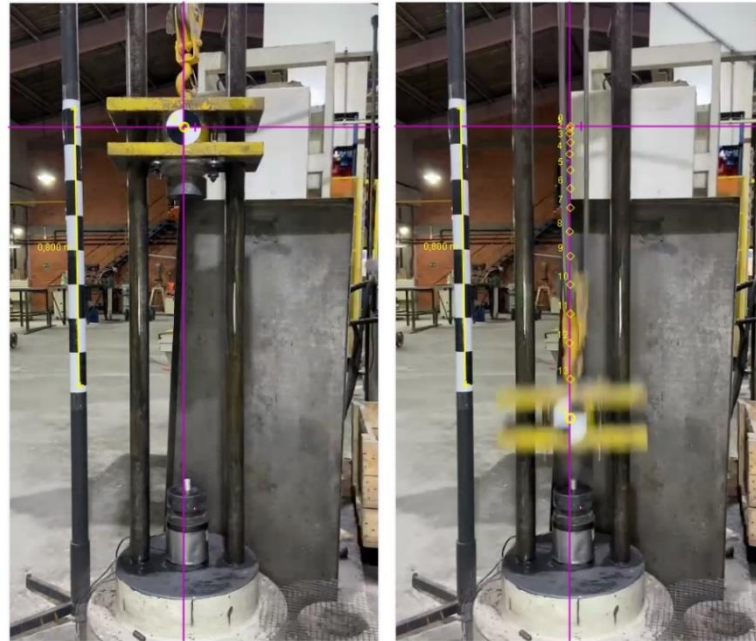


Fig. 4. Image analysis of the process

The action of the hammer can be interpreted as free-fall motion. Free-fall motion of an object occurs when the object is released from a certain height and is accelerated solely by gravitational force. In this case, the initial velocity ( $V_0$ ) of the object is zero, and the acceleration due to gravity ( $g$ ) is the only acting force. Thus, the velocity can be mathematically expressed over time by Equation 2:

$$V = V_0 + (a \cdot t) \rightarrow V = (g \cdot t) \quad (2)$$

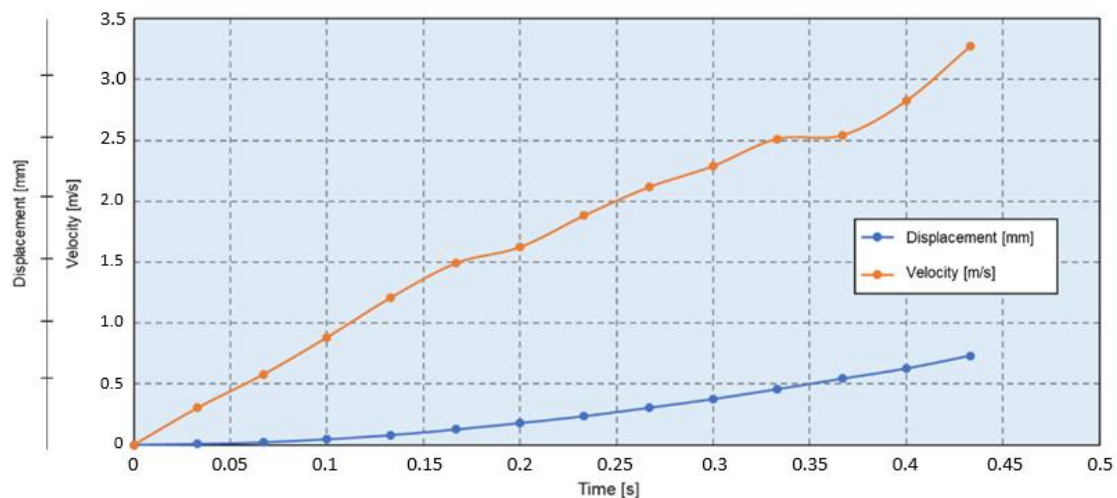


Fig. 5. Velocity and displacement data obtained during the hammer fall

The theoretical values obtained from Equation 2 are compared with the velocity data

recorded during the experiments in Figure 6. The calculated and experimentally obtained values showed good correlation up to approximately 1.5 s. From this point, the discrepancy between the curves steadily increases until the moment when the hammer touches the surface of the billet (0.433 s). At this point, the difference between the data is maximum, reaching 23%. The calculated maximum velocity was 4.2 m/s, while the experimental maximum velocity was 3.271 m/s. This difference is related to the mechanical losses that occur during the hammer movement, associated, for example, with friction between the columns. Since Equation 4 considers ideal working conditions, these losses are not taken into account in the theoretical calculations. For this reason, the theoretical velocity is higher than the one observed experimentally.

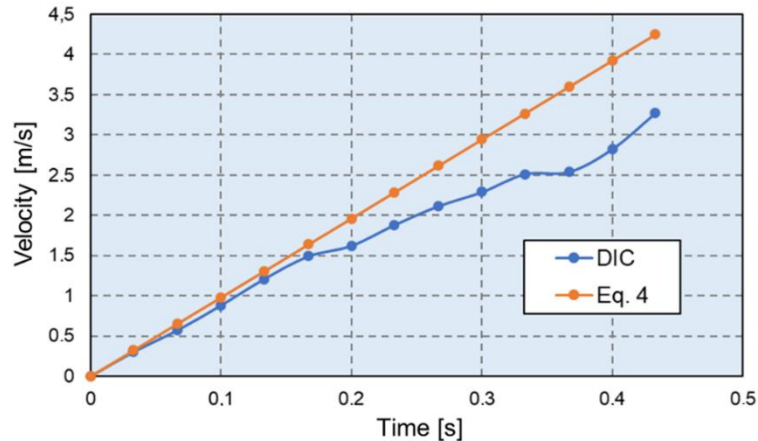


Fig. 6. Hammer fall velocity values

Figure 7 shows the variation of acceleration over time during the hammer fall obtained via DIC. The acceleration exhibits significant fluctuations, deviating from the value of gravitational acceleration at various moments. As mentioned earlier, mechanical losses, such as friction, deviate the hammer's movement from its ideal behavior. These losses restrict the falling motion, and consequently, values lower than the gravitational acceleration are observed.

As shown in Figures 6 and 7, the effect of mechanical losses is small at the beginning of the hammer's motion but intensifies as the drop progresses. This behavior has been observed by other researchers [6].

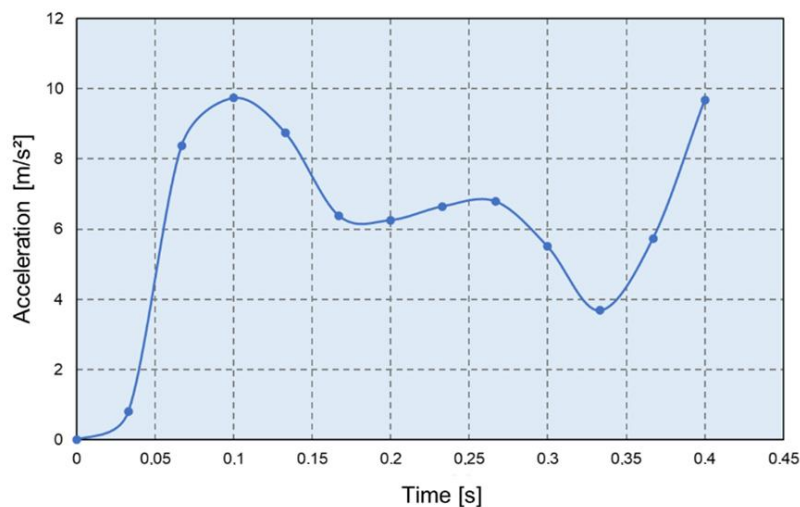


Fig. 7. Hammer acceleration during the fall

A drop hammer converts gravitational potential energy into kinetic energy as it falls. The total energy of the impact ( $E_T$ ) is equal to the kinetic energy, as indicated by Equation 3.

$$E_T = \frac{1}{2} m_i V_i^2 = \frac{G_i}{2gV_i^2} = G_i H \quad (3)$$

Where  $m_i$  represents the sum of the mass of all moving elements,  $V_i$  is the initial velocity of the hammer,  $G_i$  is the sum of the weight of all moving elements,  $g$  is the acceleration due to gravity, and  $H$  is the height of the fall.

With a hammer fall height of 0.732 m and a mass of the upper hammer system of 40 kg (considering the acceleration due to gravity ( $g = 9.81m/s^2$ ), it is possible to calculate the ideal value of the hammer's total impact energy ( $E_T = 287 J$ ), disregarding losses that occur during the hammer fall.

Due to losses associated with environmental noise and vibration in the process, only a portion of the total energy ( $E_T$ ) of the hammer is converted into useful energy ( $E_A$ ). This is the portion of energy available for deformation. Using Equation 3 and experimental data on acceleration and velocity, the values of available energy ( $E_A$ ) during the hammer fall can be defined.

Figure 8 shows the evolution of total energy ( $E_T$ ) and available energy ( $E_A$ ) as a function of time. The blue curve represents the ideal total energy, while the orange curve represents the available energy obtained during the experiment.

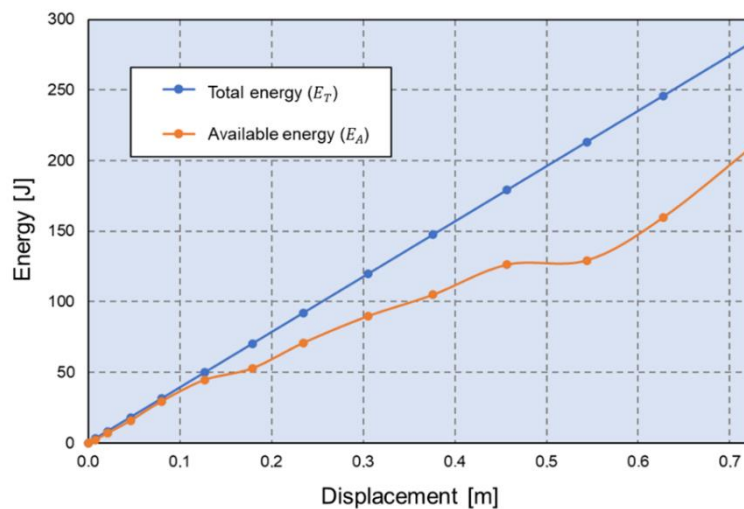
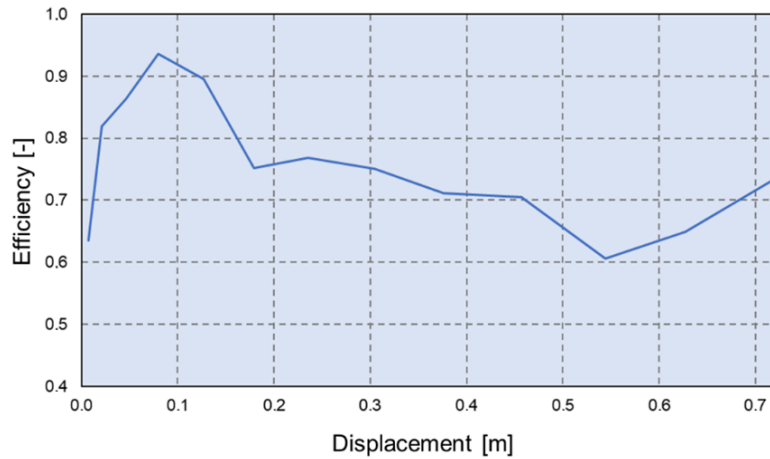


Fig. 8. Impact energy

Figure 9 shows the efficiency of the impact ( $\eta$ ) of the drop hammer. The impact efficiency is measured by the ratio  $E_A/E_T$ . The observed values range from 0.61 to 0.93, with an average value of 0.76. This value is close to reference values found in the literature for hammers with similar characteristics to those used in this study. Efficiency values between 0.8 and 0.9 are typical of light impacts, involving small load and large displacement. While values between 0.2 and 0.5 are characteristic of impacts considered heavy due to high load and small displacement.

The data obtained through image analysis in STEP I were used as input data in the finite element software to perform the numerical analysis in STEP II.



**Fig. 9.** Hammer efficiency

The billet strain during the hammer impact recorded by the high-speed camera is shown in Figure 10. The entire event occurred in just 6 ms, and a displacement of 9.7 mm was observed, resulting in a 40% reduction in the specimen's height. The average equivalent strain was calculated for each frame shown in Figure 12 with the assistance of the ImageJ© program, using Equation 4.

$$\varphi_{-eqEXP} = \ln \frac{h}{h_0} \quad (4)$$

Where  $h_0$  is the initial height, and  $h$  is the instantaneous height of the specimen.

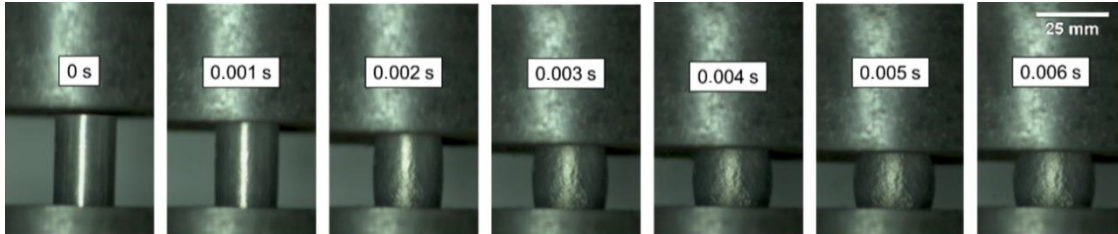


**Fig. 10.** Recording of the billet deformation during the hammer impact.

Additionally, numerical models were created to simulate the upsetting process. Figure 11 depicts the evolution of the distribution of equivalent strain throughout the process. Figure 11 also illustrates the values of the average equivalent strain obtained by finite element analysis ( $\varphi_{-eqFEM}$ ) and the average equivalent strain obtained experimentally ( $\varphi_{-eqEXP}$ ). The experimental and simulated values showed an excellent correlation with a maximum deviation of only 6.7%.

Another extremely relevant parameter in the hot forging process with a significant influence on the final properties of the forged piece is the strain rate ( $\dot{\varphi}$ ). At high temperatures, recovery and recrystallization processes occur in the material. The concomitant change in the arrangement of dislocations leads to a softening of the material. However, this process takes time, which is reduced as the strain rate increases. This means that as  $\dot{\varphi}$  increases, there is less and less time available for recovery and recrystallization processes, indicating that the yield stress depends on the material strain rate during hot forming.

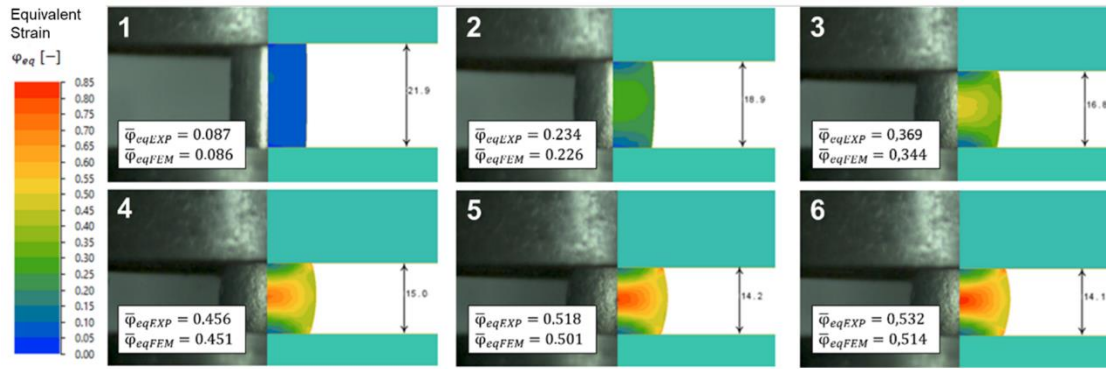


Fig. 11. Comparative framework between the strain values obtained in experiments and numerical models

Strain rate is defined as the variation of strain with respect to the variation of time and can be mathematically expressed by:

$$\dot{\varphi} = \frac{d\varphi}{dt} \quad (5)$$

From the high-speed camera images and using Equation 5, it was possible to calculate the average strain rate developed during the upsetting process. The experimental average strain rate values are compared with the values obtained by finite element analysis in Figure 12. Experimental and numerical results for average strain rate exhibit similar behavior. Initially, the values increase until reaching the maximum value in approximately 2 ms. Both analyses recorded high strain rate values during the upsetting due to the high speed of the forging equipment. In the simulation, the maximum value was 150 1/s, while in the image analysis, the maximum value was 146 1/s. After reaching the maximum value, the strain rate gradually decreases.

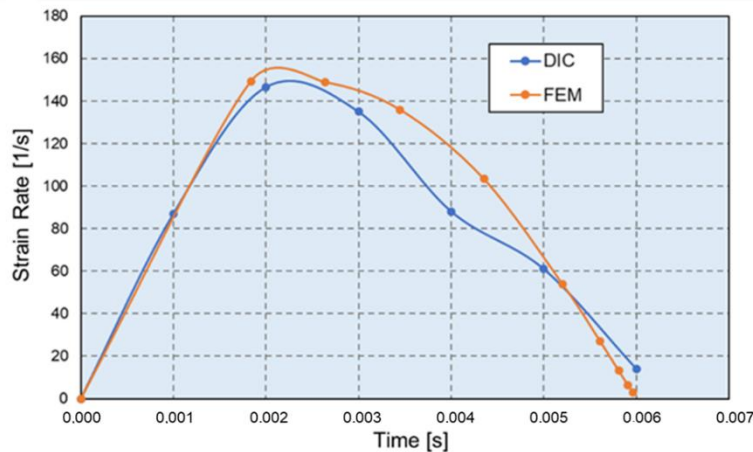


Fig. 12. Average strain rate

Temperature is one of the most crucial parameters in forming processes. Based on temperature measurements, the phenomena occurring throughout the process can be identified and analyzed. Monitoring the heating process provides various details about the heat transfer developed during the process, enhancing the understanding of the developed phenomena. Forging temperature distributions constitute boundary and input data for various analytical and numerical modeling.

Figure 13 shows thermographic images and the thermal history of the analyzed forging

process. During deformation (highlighted), an increase in temperature in the work material is observed. In the forging process, two phenomena strongly influence the temperature: heat transfer between the tools and the billet, and the heat increase associated with the forming work. Due to the high speed of the forging machine, the contact time between the tools and the billet is extremely short. In contrast, the high deformation speed developed in the process requires more work to be done. Thus, the portion of energy in the form of heat resulting from the forming is significantly greater than the energy loss associated with heat transfer. This is the reason for the observed temperature gain. This behavior was also observed by Yoneyama et al. (2018), who used an infrared thermographic camera to monitor the temperature during the hot forging of a steel alloy using a pneumatic hammer.

Non-contact temperature measurements, using thermal imaging cameras, are increasingly common in industrial practice due to technical progress in electronics and the introduction of digital technology. These devices are extremely easy to use and provide continuous visualization of results; however, they are limited to measuring the surface temperature of objects [10,11]. Nevertheless, if visual measurements are combined with numerical modeling, complementary results can be achieved, such as the temperature distribution in the core of the workpiece. Figure 13 compares the surface temperature data of the forging sample obtained numerically and through image analysis. The curves converge almost perfectly, validating the use of numerical simulation to complement experimental results with adequate precision.

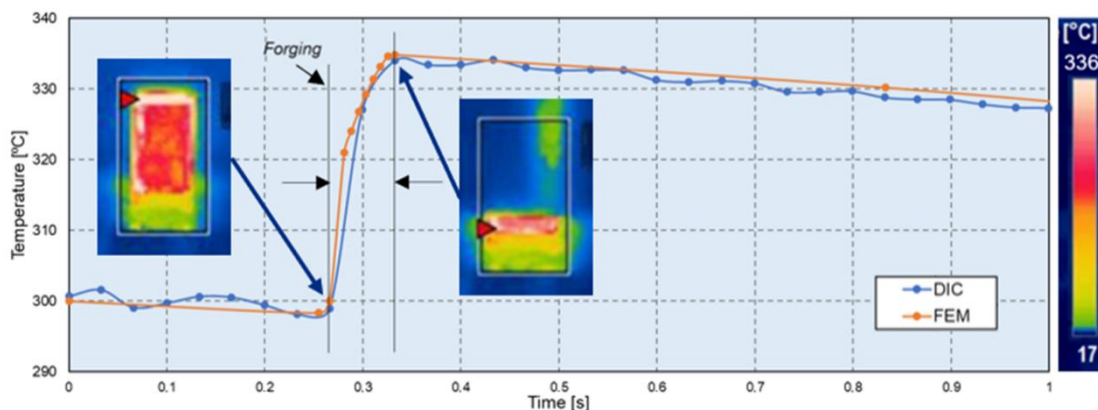


Fig. 13. Comparative of the temperature values of the forging samples

In this study, the hot forging of an aluminum alloy was investigated. However, it is important to note that using thermography in steel requires greater care. One of the biggest challenges in optical temperature measurement in steel forging processes is surface oxidation. The emissivity, i.e., the surface's ability to emit radiation, changes drastically with the formation of surface oxides. To minimize surface influences, the use of modern ratio pyrometers is recommended, which measure radiation at two wavelengths and determine the temperature from the ratio of the two radiation intensities.

In the milliseconds required for a forging operation, there are few process variables that can be measured and collected directly related to the process condition. Force is one of these few variables [12]. Force is a dependent variable whose magnitude is derived from the independent variables of the forging process. Consequently, changes in force signals reflect variations in the process due to instabilities such as geometric changes in tools or workpieces, alterations in lubrication conditions, etc.

Figure 14 compares the force data acquired during the forging operation through the load cell, numerical simulation, and image analysis. The curves exhibit analogous behavior, with the maximum force values obtained showing a discrepancy of less than 5%. Verifying the

maximum values of a cycle of signals is one of the most commonly employed monitoring features [13-15].

The force data obtained by DIC were calculated using the rheological properties of the material (Table 1). The material's yield curve depends heavily on deformation, strain rate, and temperature. Thus, the data obtained via DIC for these variables were inserted into the equation describing the material's mechanical behavior at high temperatures. The results validate the use of DIC to monitor forming force in high-speed processes as analyzed.

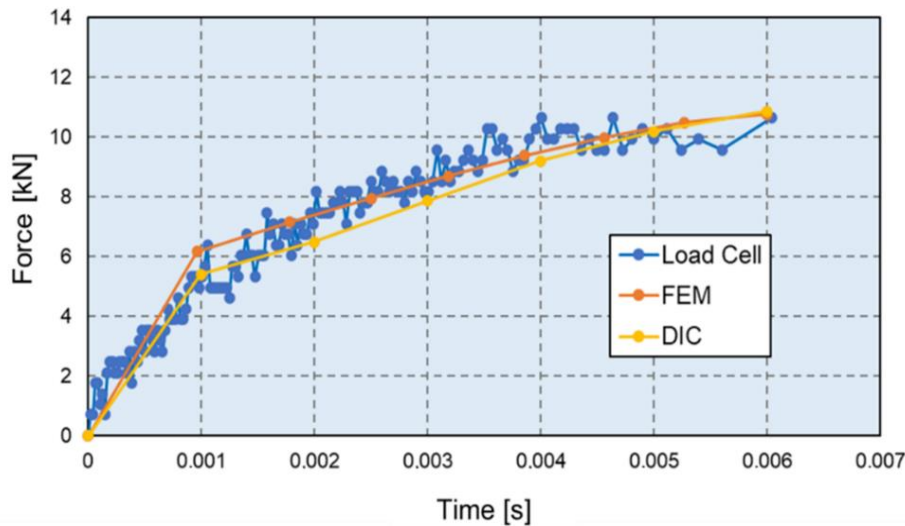


Fig. 14. Force values

## DISCUSSION

This work introduces an approach for monitoring the hot forging process using image analysis techniques. A monitoring approach was proposed, involving the use of digital cameras to capture images of forging operations, followed by image processing to assess dynamic machine conditions, such as impact velocity, temperature, and energy developed during the process.

Through the analysis of images captured by the conventional camera, a comprehensive analysis of the kinetics of the forging hammer falling process (STEP I) was possible. With a low-cost setup, extremely relevant information for the control of the forming process. Several researchers have been working on developing models to determine the energy involved in hammer forging processes [16-18]. The approach presented in this work allows real-time quantification of forming energy, enabling the detection of potential variations in equipment efficiency. This makes it possible to implement appropriate measures to improve equipment performance before production losses occur due to reduced efficiency. Furthermore, accurate and real-time measurement of the hammer's position is essential for effective automatic process control [19]. This article proposes the use of a non-contact measurement system to overcome the limitations associated with the installation of detection sensors and the noise in data due to vibration and impact during the impact process.

In STEP II, DIC allowed for the quantification of strain, strain rate, temperature, and force at each instant of the process. Strain and strain rate data are crucial for understanding the metallurgical phenomena occurring during hot working. Quantifying these parameters in real-time provides extremely relevant information about the final part's quality.

Similarly, quantifying temperature during the process is crucial. Thermography is the safest way to measure temperature fields in both the workpiece and the tool during forging processes, as other methods face difficulties due to high temperatures and pose risks to operators. Precisely defining the material's emissivity and calibrating the measurement range enable the detection of precise temperature zones [20].

The DIC data obtained in STEP I and STEP II were used as input data in finite element software. Numerical simulations served as complementary data sources to the image analysis conducted during forming. This bilateral exchange of information between the physical world and a digital realm forms the basic structure of digital twins [21]. The physical world includes devices associated with various data acquisition instruments. The acquired data are transmitted to the virtual space where they are analyzed to monitor the process. Through the information generated by DIC, it is possible to anticipate potential future states and improve resource management throughout the production cycle.

Virtual technologies are extremely useful in meeting the increasingly stringent requirements of modern industry. Their application can significantly reduce product development time, cut costs, and prevent defects and failures in production. Virtual models of technological processes allow for evaluating the impact of design changes on product quality, contributing to the optimized use of production equipment and tools. These technologies empower engineers to make decisions through the simulation of various engineering activities, eliminating the need for expensive prototypes and physical experiments. Currently, monitoring and data collection systems are essential parts of many mechanical forming operations, serving as crucial tools to ensure production efficiency. The image analysis demonstrated in this study can accurately measure critical parameters and assess the process and machine state satisfactorily. It's important to highlight that for the application of DIC, the imaging acquisition system must be properly configured. The camera should be positioned in a secure location where the desired information can be captured. Additionally, a calibration method must be used. When integrated with signal processing and machine learning algorithms, it provides valuable predictions regarding tool and machine maintenance, as well as offering guidance to ensure safe operation and other significant benefits.

## CONCLUSIONS

In conclusion, the article presents a approach to monitoring the hot forging process with a drop hammer, based on the use of image analysis techniques. It was observed that the hammer's speed decreases before contact between the die and the workpiece. The measured speed is 23% lower than the theoretical speed (without mechanical losses). The hammer's efficiency increases at the beginning of the fall, reaching a maximum value of 93% after a displacement of 0.08 m. As the tool's movement progresses, the efficiency drops to 61%. The results suggest that image analysis is an effective tool for improving the efficiency of the hot forging process and ensuring the quality of forged products.

The use of this methodology allowed for the monitoring and analysis of the forging process, and its implementation enables future integration with process analysis and control systems, serving as a means of data acquisition for use in Industry 4.0 technologies. Through the approach presented in this work, it's possible to calculate process parameters in milliseconds without the need for numerical simulations, which require longer computation times. The methodology even allowed such implementation to be possible in outdated equipment, providing a low-cost alternative.

## ACKNOWLEDGEMENT

The authors thank CNPq, CAPES and FAPERGS for financial support (FAPERGS/CAPES 06/2018, process: 19/2551-0000710-8);(CNPq/ MCTI/FNDCT n° 18/2021, process: 404196/2021-7);(CNPq research productivity – PQ1-4/2021; PDJ – 25/2021 150252/2022-6; GD – 2019);(CAPES (PROEX-IES-2020); and the Metalforming Laboratory (LdTM) for technical support.

### *Conflict-of-interest statement*

The authors certify that they have no affiliations with or involvement in any organization or entity with any financial interest, or non-financial interest in the subject matter or materials discussed in this manuscript.

## REFERENCES

1. Semiatin S.L., ASM Handbook, Metalworking: Bulk Forming. vol. 14A. ASM International; 2005.
2. Altan T., Ngaile G., Shen G., Cold and Hot Forging: Fundamentals and Applications. ASM International, 2005.
3. Prasad Y., Rao K.P., Sasidhara S., Hot Working Guide-A Compendium of Processing Maps. 2<sup>a</sup> ed. ASM International; 2015.
4. Kim H., Gu J.C., Zoller L., Control of the servo-press in stamping considering the variation of the incoming material properties. International Deep Drawing Research Group, IOP Conf. Ser. Mater. Sci. Eng., 651, 2019.
5. Lins G.M., Mechatronic system for measuring hot-forged automotive parts based on image analysis. Trans. Inst. Meas. Control., 2018, Vol. 40(13) 3774–3787.
6. Saberi S., Fischer J., Stockinger M., Tikal R., Afsharmia R., Theoretical and experimental investigations of mechanical vibrations of hot hammer forging. Int. J. Adv. Manuf. Technol., 114, 3037–3045 2021.
7. Durand C., Freund L., Baudouin C., Bigot R., Guérin J., Comparison of different sensor technologies to monitor a forging process. 24th International Conference on Material Forming, 2021.
8. Hensel, A., Spittel, T., Kraft – und Arbeitsbedarf bildsamer Formgebungverfahren, Leipzig: VEB Deutscher Verlag für Grundstoffindustrie, 1978.
9. Marques A.S., Costa L.L., Dalcin R.L, Brito A.M.G, Schaeffer L., Rocha A.S., Optimizing hot forging process parameters of hollow parts using tubular and cylindrical workpiece: numerical analysis and experimental validation. J. Mech. Eng. Autom., 2018.
10. Yoneyama T., Miyoshi K., Tate T., Contact stress and temperature during air-stamp hammer upsetting of a circular cylinder. J. Manuf. Proc., 32, 2018.
11. Hawryluk M., Ziemba J., Possibilities of application measurement techniques in hot die forging Processes. Measurement, 2017.
12. Rasmussen, S.F., Tonnage Monitoring for Mechanical Forging Presses, FORGE Magazine, 2010.
13. Grogan, R., High Speed Stamping Process Improvement Through Force and Displacement Monitoring. Helm Instrument Company Technical Report, 2002.
14. Knussmann, K. D., And Rose, C., Signature-Based Process Control (SbPC™), Signature Technologies Technical Report, pp. 311–325, 1993.

15. Auto Body Consortium, Total Tonnage Signature Decomposition for a Transfer/Progressive Die Process Analysis of Station-by-Station Test at A. J. Rose 250 Ton Press, NIST Advanced Manufacturing Program: NZS Technical Report No. NZS-204, 1997.
16. Zhang, Y.; Liu, F. The research of hydraulic control system for die forging hammer. *China Met. Form. Equip. Manuf. Technol.* 2010, 1, 68–71.
17. Jin, W.; Ma, W.; Yang, S. Simulation Research on Impact Energy of 50kJ Hydraulic Die Forging Hammer. *Met. Equip. Manuf. Technol.* 2008, 5, 90–92.
18. Zhang, X.; Li, W.; Li, S. Forging process optimization of precision closed die forging hammer. *MW Met. Form.* 2018, 11, 76–77.
19. Yan, X.; Chen, B. Analysis of a Novel Automatic Control Approach for the Free Forging Hammer. *Appl. Sci.* 2020, 10, 9127.
20. Popovoc M., Mandic V., Delic M., Pavicevic V., Experimental-Numerical Analysis of Hot Forging Process with Monitoring of Heat Effects, *New Technologies, Development and Application IV*, Springer, 2021.
21. Jones D., Snider C., Nassehi A., Yon J., Hicks B., Characterising the digital twin: A systematic literature review. *CIRP J. Manuf. Sci. Technol.*, vol. 29, pp. 36–52, 2020.